REPORT

JUPITER

The depth of Jupiter's Great Red Spot constrained by Juno gravity overflights

Marzia Parisi[1]*, Yohai Kaspi[2], Eli Galanti[2], Daniele Durante[3], Scott J. Bolton[4], Steven M. Levin[1], Dustin R. Buccino[1], Leigh N. Fletcher[5], William M. Folkner[1], Tristan Guillot[6], Ravit Helled[7], Luciano Iess[3], Cheng Li[8]†, Kamal Oudrhiri[1], Michael H. Wong[8,9]

Jupiter's Great Red Spot (GRS) is the largest atmospheric vortex in the Solar System and has been observed for at least two centuries. It has been unclear how deep the vortex extends beneath its visible cloud tops. We examined the gravity signature of the GRS using data from 12 encounters of the Juno spacecraft with the planet, including two direct overflights of the vortex. Localized density anomalies due to the presence of the GRS caused a shift in the spacecraft line-of-sight velocity. Using two different approaches to infer the GRS depth, which yielded consistent results, we conclude that the GRS is contained within the upper 500 kilometers of Jupiter's atmosphere.

Jupiter's Great Red Spot (GRS) is a large and enduring anticyclonic storm in Jupiter's atmosphere. Both its size (currently more than 16,000 km east-west) and centuries-old longevity are unlike other vortices in the Solar System and must be driven by the underlying dynamics of the storm. It is unknown whether the vortex is deep-rooted in the surrounding zonal flows (east-west bands), or whether a shallow system can maintain such a long-living storm (*1*, *2*). Spacecraft gravity measurements are sensitive to density perturbations in the deeper layers of the atmosphere, below the visible cloud level, so close encounters with the vortex provide an opportunity to study the GRS gravity signature and infer the depth of its winds.

The Juno spacecraft flew twice over the GRS, in February and July 2019, at altitudes below 20,000 km. These encounters (perijoves) were dedicated to measurements of the local gravitational field. Earlier observations of the GRS had occurred during another perijove in July 2017, during which the spacecraft attitude was optimized for Microwave Radiometer (MWR) investigations that precluded gravity measurements. The microwave observations indicated that the GRS extends down to at least 100-bar atmospheric pressure, well below the cloud level (estimated at 0.7 bar), which corresponds to a depth of ~240 km (*3*). MWR observations are complementary to gravity measurements because they provide a minimum value for the vortex's vertical extension (*3*). Previous Juno gravity measurements have shown that Jupiter's gravity field is hemispherically asymmetric (*4*), which has been explained by the powerful zonal winds in which the GRS is embedded (*5*). By relating the observed cloud-level winds to the gravity measurements, the depth of the jet streams has been estimated at 3000 km (*6*). This estimate assumed thermal wind balance, which is expected to dominate vorticity balance on large, rapidly rotating planets (*6*). However, it remains unclear how far down the GRS winds extend between the surrounding jet streams.

Before Juno arrived at Jupiter, Parisi *et al.* proposed to use gravity data to determine the depth of the GRS (*7*) by determining the planet's longitudinally dependent gravity field. Later on, an alternative proposal suggested the use of a Slepian basis set (*8*), whose functions are defined as linear combinations of spherical harmonics chosen to maximize the information in a selected domain. The Slepian approach has previously been used to describe localized features on Earth (*9*, *10*) and to analyze incomplete data collected over a limited area (*11*). Simulations predicted that the gravity signal of the GRS could potentially be described with a single Slepian coefficient, and that the gravity data would be sensitive to the depth of the GRS if it was at least a few hundred kilometers (*8*). Similar predictions were reached using a complementary approach that models the GRS as a vertical dipole of mass concentrations (mascons), which estimates the mass of the anomalies directly (*12*).

Juno's orbit around Jupiter is quasi-polar and highly eccentric, with the spacecraft descending to altitudes of about 3500 km over Jupiter's cloud tops every 53 days, sweeping the planet from its north pole to its south pole within a couple of hours (*13*). The oblateness of the planet causes a northward shift of the perijove latitude by ~1° per orbit, from an initial latitude of 4°N. Therefore, the spacecraft observes the GRS (20°S) from an increasing distance as the mission proceeds. During gravity passes, two-way Doppler measurements of the spacecraft range rate are performed using coherent radio links with NASA's Deep Space Network in X-band (~8 GHz) and Ka-band (~32 GHz) (*14*), which are sensitive to perturbations in the gravity field of Jupiter. We analyzed data from 12 Juno perijoves (PJs) labeled with progressive numbers 1, 3, 6, 8, 10, 11, 13, 14, 15, 17, 18, and 21. We initialized Jupiter's global gravity field and tidal response using Juno gravity data up to PJ17 (*15*), to which we added the GRS overflights data from PJ18 and PJ21. Figure 1 shows the Juno tracks over Jupiter's reference surface during the PJ18 and PJ21 passes.

We combined the Juno gravity measurements using a least-squares multiarc filter implemented in the orbit determination software MONTE (*16*), which was also used for trajectory integration and data analysis. The range-rate integration time was 60 s and the typical noise RMS (root mean square) was between 5 and 10 $\mu m\ s^{-1}$ (one-way). The filter requires the accurate reconstruction of the Juno trajectory, including every acceleration acting on the spacecraft, both gravitational and nongravitational (*4*, *15*). We searched for the GRS gravity signature in the Juno overflight data by processing the range-rate residuals while solving for the zonal gravity field of Jupiter. Previous analyses (*15*) have discussed the difficulty of fitting the Juno range-rate data from multiple perijoves without allowing for longitudinal or temporal variations of the gravity field.

The range-rate residuals for PJ18 and PJ21, after removing the effect of the zonal gravity field, show non-negligible signals over time scales of ±1 hour around closest approach to Jupiter (Fig. 2, A and C). These deviations from zonal symmetry can be removed by the addition of short-lasting, constant accelerations (*15*) but could also be partly attributed to the GRS. The closest approaches to Jupiter occurred at latitudes around 20°N; Juno crossed the GRS latitude 20°S about 20 min later. We analyzed the remaining non–axially symmetric, nonstatic signatures on the range-rate residuals after removing the effect of the zonal gravity field of Jupiter. Our objective was to isolate the longitudinal or temporal effects, which include the signal from the GRS.

The measured PJ18 residuals (Fig. 2A) show deviations from the mean value ~10 min before perijove (latitude ~30°N). We do not expect

[1]Jet Propulsion Laboratory, California Institute of Technology, Pasadena, CA 91109, USA. [2]Department of Earth and Planetary Sciences, Weizmann Institute of Science, Rehovot 76100, Israel. [3]Department of Mechanical and Aerospace Engineering, Sapienza University of Rome, 00184 Rome Italy. [4]Southwest Research Institute, San Antonio, TX 78238, USA. [5]School of Physics and Astronomy, University of Leicester, Leicester LE1 7RH, UK. [6]Université Côte d'Azur, Observatoire de la Côte d'Azur, Laboratoire Lagrange, Centre National de la Recherche Scientifique, 06304 Nice, France. [7]Center for Theoretical Astrophysics and Cosmology, Institute for Computational Science, University of Zurich, 8057 Zurich, Switzerland. [8]Department of Astronomy, University of California, Berkeley, CA 94720, USA. [9]Carl Sagan Center for Research, SETI Institute, Mountain View, CA 94043, USA.
***Corresponding author. Email: marzia.parisi@jpl.nasa.gov**
†Present address: Department of Climate and Space Sciences and Engineering, University of Michigan, Ann Arbor, MI 48109, USA.

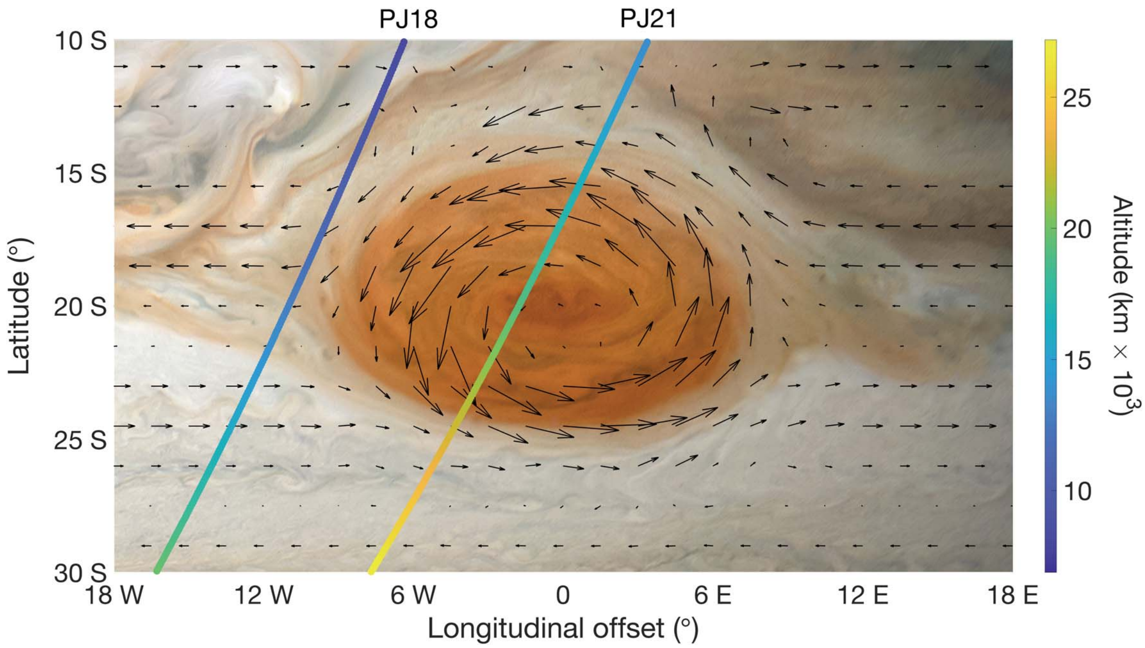

Fig. 1. Geometry of the Juno GRS gravity observations. The GRS velocity field (black arrows) at the time of PJ21 (*20*, *32*) with Juno tracks during PJ18 and PJ21 (gradient lines) is superimposed on JunoCam imaging of the GRS during PJ21 (*33*). The spacecraft altitude during the GRS closest approach (latitude 20°S) was 13,000 km during PJ18 and 19,000 km during PJ21, with eastward longitudinal offsets of 11° and 2°, respectively. [Background image credit: NASA/JPL-Caltech/SwRI/MSSS/Kevin M. Gill © CC BY, released under the Creative Commons Attribution 3.0 Unported (CC BY 3.0) license https://creative-commons.org/licenses/by/3.0/legalcode]

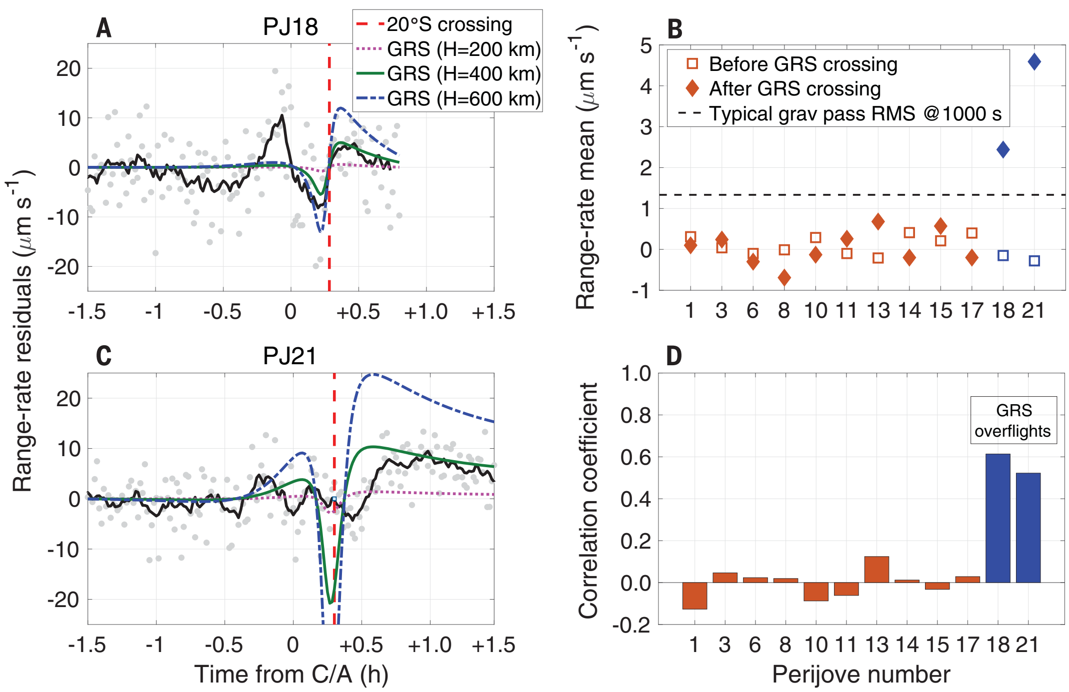

Fig. 2. Nonzonal, nonstatic effects on the range-rate residuals from PJ18 and PJ21. (**A** and **C**) PJ18 (A) and PJ21 (C) range-rate residuals (gray dots) with their 10-min moving average (black solid line), for the period ±1.5 hours around closest approach (C/A) to Jupiter. The red dashed vertical line marks the GRS crossing (20°S) by the spacecraft track. The other lines represent the expected gravity signal from the GRS for different depths, as indicated. (**B**) Range-rate mean values (Δv), before (squares) and after (diamonds) the crossing of latitude 20°S, for all perijoves with gravity measurements. (**D**) Correlation coefficients between the predicted GRS gravity signal (for H = 300 km) and the moving average of the residuals. In (C) and (D), non-GRS perijoves are orange; GRS overflights are blue.

these fluctuations to be related to the GRS, as the spacecraft was then ~100,000 km away. Figure 2A also shows the expected gravity signal from the GRS, assuming that the cloud-level winds decay at a depth H. The correlation between the predicted GRS signature and the smoothed residuals is shown in Fig. 2D.

PJ21 data (Fig. 2C) also show correlation with the GRS signal, with a constant shift in the line-of-sight velocity of ~5 μm s^{-1}, lasting until at least 1.5 hours after perijove. This behavior is typical of passing one or more mass concentrations, such as those associated to the GRS. The long duration of the constant shift favors decoupling of the constant accelerations applied around perijove from the GRS signal. We interpret the temporal offset between the negative peaks around the GRS crossing (measured versus predicted) as due to unrelated nonzonal effects. We investigated the role of the accelerations in removing the excess longitudinal and/or temporal signatures and aliasing with the GRS parameters (*17*). After compensating for the estimated accelerations (fig. S7, C and D), we found that (i) most of the remaining range-rate signal can be explained by concentrated masses at the GRS location, and (ii) unexplained nonzonal effects (*15*) can cause the offset between the PJ21 range-rate residuals and the predicted GRS signal (Fig. 2C).

The average velocity shift (Δv) in the residuals before and after the crossing of latitude 20°S, for all perijoves, is shown in Fig. 2B. These averages were calculated over time periods of 0.5 to 1.5 hours. Passes over the GRS show shifts of a few $\mu m\ s^{-1}$, above the typical noise RMS for integration times exceeding 1000 s (*17*). Conversely, the velocity profiles for perijoves away from the GRS do not show deviations from the mean. The magnitude of the offset on the range-rate data contains direct information on the GRS depth (*17*), which is reflected in the output parameters of the least-squares solution used to infer the vertical extent of the winds.

Figure 2D shows the correlation coefficients between the predicted GRS gravity signal for H = 300 km and the moving average of the range-rate residuals, for all 12 perijoves (*17*). The non-GRS passes are characterized by very low correlations of less than 10%, whereas the correlations for PJ18 and PJ21 are 50 to 60%. Although the signal-to-noise ratio is low, perijoves 18 and 21 differ from the other passes, indicating that the GRS depth can be constrained using the Juno gravity data.

The shape of the GRS has evolved over the past several decades, with its longitudinal dimension shrinking and giving the vortex a more circular shape (*18*, *19*). We measured horizontal wind speeds in the GRS using optical data acquired about 25 days before PJ21 (*17*, *20*), taken as part of an annual Hubble Space Telescope observing program (*21*). Mean velocities measured in the high-speed ring are 106 m s^{-1}, with a standard deviation of 11 m s^{-1}. Remote observations provide information about the surface dynamics of the zonal winds and the vortex, but little is known about the dynamics below the cloud level. The surrounding jets extend very deep (*6*), which confines the latitudinal extent and direction of the GRS circulation. We therefore assume that the vortex preserves its shape until it decays below the depth H. For simplicity we consider a hyperbolic tangent decay function, assumed to decay rather sharply within 100 km around H (*22*, *23*), but our results are robust to other choices of the decay shape (*17*). Because the planet is rapidly rotating and the dynamics are geostrophic (to leading order), thermal wind balance can be used to calculate the density anomalies balancing the vortex velocity (*24*). The applicability of this approach to modeling Jupiter's atmosphere has been discussed elsewhere (*25*, *26*). Unlike Earth's atmospheric vortices (*27*), the local centripetal force can be neglected.

The predicted density anomalies associated with the GRS for a sample depth H = 300 km are shown in Fig. 3A. The density profile resembles a dipole, with a positive mascon in the upper levels [with gravitational parameter GM_A (where G is the gravitational constant and M_A is the positive mass anomaly)] and a negative mascon at depth (with parameter GM_B, where M_B is the negative mass anomaly). The sum of the two masses is zero, to first order (*17*). The relationship between the mass and the separation between the positive and negative anomaly is injective (fig. S3); therefore, the depth (H) can be inferred by using MONTE to estimate the mass (*12*). In the orbit determination software, we model the vortex as a pair of flat disk mascons, whose masses are constrained to be equal and opposite in sign. Deeper winds entail a larger mass involved in the circulation of the GRS and an increasing vertical distance between the mascons. A sign inversion between the upper and deeper levels was also observed in MWR measurements during PJ7 (*3*).

An alternative approach to searching for the GRS gravity signature is to use Slepian functions to characterize the wind-induced, concentrated surface gravity anomalies (*8*). Figure 3B shows that the GRS predicted gravity disturbances form a north-south dipole. The Slepian functions are defined within the bounded domain delimited by an ellipsoid centered at the GRS location spanning 20° in latitude and 30° in longitude. Our analysis of the Slepian functions (*17*) shows that a single function, labeled $\mathbf{g}_2$, can describe the gravity perturbations generated by the GRS, to leading order (*8*). The magnitude of the corresponding Slepian coefficient α_2 increases with the depth of the GRS (Fig. 4B); therefore, the depth (H) can be inferred from a measurement of α_2.

To account for unmodeled accelerations (Fig. 2, A and C), we introduced small constant accelerations, each of 10-min duration, for ±1 hour around perijove (*15*, *28*). In addition to standard estimated parameters, such as Jupiter's zonal gravity field and pole position (*17*), we also added one coefficient specific to the determination of the depth of the GRS: the gravitational parameter of the positive disk mascon GM_A for the mascon approach, or the Slepian coefficient α_2 for the Slepian approach. Both parameters were allowed to vary without constraint.

The results of the mascon analysis are shown in Fig. 4A. The dipole structure is implemented in MONTE, and the vertical separation affects both the estimated central value of GM_A and its formal uncertainty (*12*). We measure GM_A = 1.47 (±1.08) × 10^{-1} $km^3\ s^{-2}$ (all uncertainties are 1σ). The derived GRS depth is then obtained from the predicted relationship between H and GM_A from thermal wind balance, finding $H = 290^{+85}_{-140}$ km. For the Slepian approach (Fig. 4B), the estimated α_2 coefficient is 3.7 (±2.4) × 10^{-5}, which implies that the winds extend down to $H = 310^{+60}_{-90}$ km. The two different methods give consistent solutions for the depth of the GRS and are compatible with the depth inferred from the MWR observations (*3*). We tested the stability of both solutions against different models of the unknown nonzonal, nonstatic effects, which indicated that the estimated depth is robust (*17*).

Both methods assume that the GRS is in thermal wind balance, and each has strengths and limitations, which are complementary to one another (*12*, *17*). They differ in the way the predicted density profile is used: either to model mass concentrations or to model the gravitational potential at the spacecraft altitude. They provide consistent results and indicate (Fig. 4) a 3σ upper limit on the GRS depth of 500 km (750 bar). This upper limit is compatible with laboratory analog experiments and

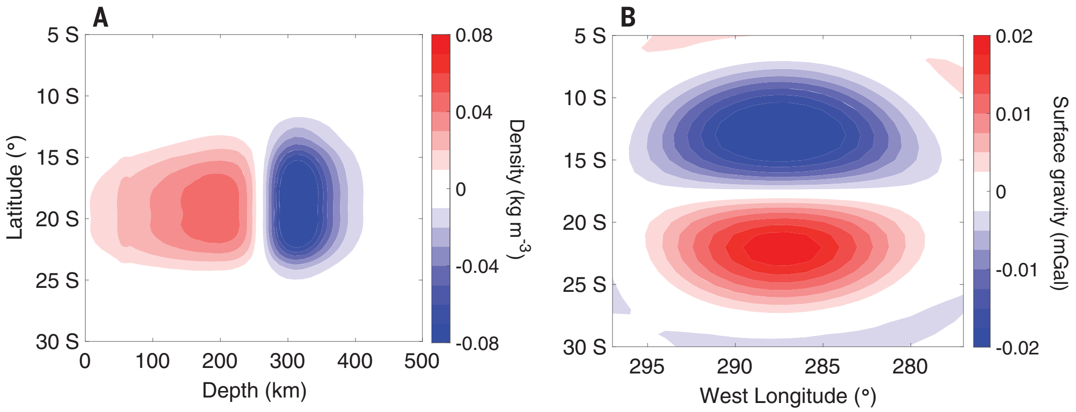

Fig. 3. The predicted signal for a 300-km-deep GRS, assuming thermal wind balance. (**A**) Density anomalies as a function of depth and latitude, for a transversal section taken at the longitude passing through the GRS center at the time of the velocity measurements (*17*, *20*, *32*). (**B**) Surface gravity anomalies as a function of longitude and latitude.

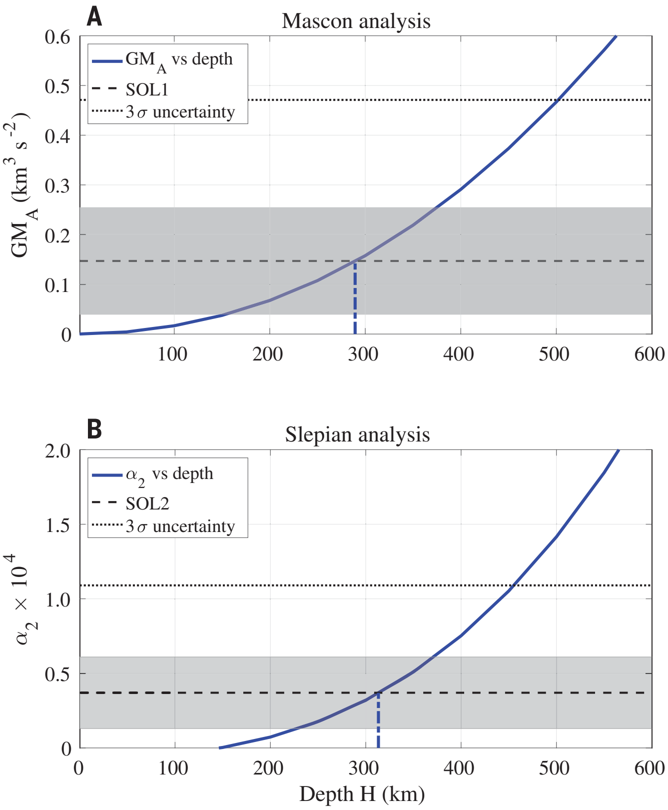

Fig. 4. Results of the GRS depth estimation. (**A**) Results of the mascon approach (best-fitting value labeled SOL1), shown with the predicted relationship between H and GM_A assuming thermal wind balance (blue). (**B**) Results of the Slepian approach (SOL2) shown with the relationship between H and α_2 for the predicted gravity anomalies (blue). In both panels, the estimated value is shown with its 1σ uncertainty (gray shaded area) and the 3σ upper limit (dotted horizontal line).

numerical simulations (*29*, *30*). With 1σ uncertainty, we find that the GRS is ~300 ± 100 km deep. However, the minimum depth of the GRS is not well constrained by our analysis. This was expected, because the GRS gravity signal is only 5% as strong as the background zonal wind signal (*4*, *15*). Our use of random accelerations de-weights the Doppler data and increases the formal uncertainties. However, Juno MWR observations provide a minimum value for the vortex's vertical extension of ~240 km (*3*), which complements our gravity measurements. Although it is possible that the GRS winds still increase below the cloud level (*31*), before they begin decaying deeper down, any increase must be less than 50% of the cloud-level velocity, otherwise the inferred depth would be shallower than indicated by MWR. We therefore conclude that the depth of the GRS is between 200 and 500 km.

Our results suggest that the GRS is much shallower than the surrounding zonal jets, which have depths of ~3000 km (*6*). The GRS is nonetheless deeply rooted, extending far below the cloud level at 0.7 bar and well beyond the water condensation level (~80 km beneath the cloud level) (*31*). Although Jupiter does not have a solid surface, the GRS is still shallow in terms of the aspect ratio between the vertical and horizontal scales (~1/200 or 0.5%). This is even shallower than Earth's cyclones and anticyclones, which have typical ratios of 1 to 4%, limited by the depth of Earth's troposphere. The driving mechanisms for Earth's vortices are very different, with roles played by atmospheric instability processes and the solid surface, the latter not being present on Jupiter. It remains unclear why the GRS has a depth of only a few hundred kilometers while the surrounding jets, which power the GRS, extend much deeper. However, a shallow GRS is consistent with its change in size over the past several decades (*19*).

REFERENCES AND NOTES

1. T. E. Dowling, A. P. Ingersoll, *J. Atmos. Sci.* **46**, 3256–3278 (1989).
2. J. Yano, G. R. Flierl, *Ann. Geophys.* **12**, 1–18 (1994).
3. S. J. Bolton *et al.*, *Science* 10.1126/science.abf1015 (2021).
4. L. Iess *et al.*, *Nature* **555**, 220–222 (2018).
5. Y. Kaspi, *Geophys. Res. Lett.* **40**, 676–680 (2013).
6. Y. Kaspi *et al.*, *Nature* **555**, 223–226 (2018).
7. M. Parisi, E. Galanti, S. Finocchiaro, L. Iess, Y. Kaspi, *Icarus* **267**, 232–242 (2016).
8. E. Galanti *et al.*, *Astrophys. J. Lett.* **874**, L24 (2019).
9. C. Harig, F. J. Simons, *Proc. Natl. Acad. Sci. U.S.A.* **109**, 19934–19937 (2012).
10. F. J. Simons, F. A. Dahlen, M. A. Wieczorek, *SIAM Rev.* **48**, 504–536 (2006).
11. F. J. Simons, F. A. Dahlen, *Geophys. J. Int.* **166**, 1039–1061 (2006).
12. M. Parisi *et al.*, *Planet. Space Sci.* **181**, 104781 (2020).
13. S. J. Bolton *et al.*, *Science* **356**, 821–825 (2017).
14. S. W. Asmar *et al.*, *Space Sci. Rev.* **213**, 205–218 (2017).
15. D. Durante *et al.*, *Geophys. Res. Lett.* **47**, e2019GL086572 (2020).
16. S. Evans *et al.*, *CEAS Space J.* **10**, 79–86 (2018).
17. See supplementary materials.
18. A. A. Simon *et al.*, *Astron. J.* **155**, 151 (2018).
19. A. Sánchez-Lavega *et al.*, *Astron. J.* **156**, 162 (2018).
20. M. H. Wong *et al.*, *Geophys. Res. Lett.* **48**, e2021GL093982 (2021).
21. A. A. Simon, M. H. Wong, G. Orton, *Astrophys. J.* **812**, 55 (2015).
22. E. Galanti *et al.*, *Geophys. Res. Lett.* **46**, 616–624 (2019).
23. Y. Kaspi *et al.*, *Space Sci. Rev.* **216**, 84 (2020).
24. Y. Kaspi, W. B. Hubbard, A. P. Showman, G. R. Flierl, *Geophys. Res. Lett.* **37**, L01204 (2010).
25. K. Zhang, D. Kong, G. Schubert, *Astrophys. J.* **806**, 270 (2015).
26. E. Galanti, Y. Kaspi, E. Tziperman, *J. Fluid Mech.* **810**, 175–195 (2017).
27. J. R. Holton, *An Introduction to Dynamic Meteorology* (Elsevier/Academic Press, 2004).
28. L. Iess *et al.*, *Science* **364**, eaat2965 (2019).
29. D. Lemasquerier, G. Facchini, B. Favier, M. Le Bars, *Nat. Phys.* **16**, 695–700 (2020).
30. R. K. Yadav, M. Heimpel, J. Bloxham, *Sci. Adv.* **6**, 46 (2020).
31. L. N. Fletcher *et al.*, *Icarus* **208**, 306–328 (2010).
32. M. Wong, "Jupiter Great Red Spot Velocity Fields from HST/WFC3" (Mikulski Archive for Space Telescopes); https://doi.org/10.17909/t9-jfs3-p240.
33. K. M. Gill, "Great Red Spot, Perijove 21"; www.missionjuno.swri.edu/junocam/processing?id=7258.

ACKNOWLEDGMENTS

We thank D. J. Stevenson, A. P. Ingersoll, and the Juno Interiors and Atmospheric Working Groups for useful discussions; citizen scientist K. M. Gill, who processed the background image in Fig. 1 as part of Juno's JunoCam outreach program; and N. Gavriel for graphical assistance with Fig. 1. **Funding:** This research was carried out at the Jet Propulsion Laboratory, California Institute of Technology (M.P., S.M.L., D.R.B., W.M.F., K.O.) under contract 80NM0018D0004 with NASA; at the Weizmann Institute of Science (WIS) in Israel (Y.K. and E.G.) with support from the Israeli Space Agency and the Helen Kimmel Center for Planetary Science at WIS; at Sapienza University of Rome (D.D. and L.I.) under contract 2017-40-H.0 with the Italian Space Agency (ASI); at the Southwest Research Institute (S.J.B.) under contract to NASA; at the University of Leicester (L.N.F.) with support by a European Research Council Consolidator Grant (under the European Union's Horizon 2020 research and innovation program, grant agreement 723890); at the Observatoire de la Côte d'Azur (T.G.) under the sponsorship of the Centre National d'Etudes Spatiales; with support by the 51 Pegasi b Postdoc Fellowship sponsored by the Heising-Simons Foundation (C.L.); at UC Berkeley and the SETI Institute (M.H.W.) with support from NASA through Participating Scientist grant 80NSSC19K1265 and through the Space Telescope Science Institute (for programs GO-13937 and GO-15502), which is operated by the Association of Universities for Research in Astronomy Inc. under NASA contract NAS 5-26555. **Author contributions:** M.P. led the data analysis and interpretation of the gravity data. M.P., Y.K., and E.G. wrote the manuscript. Y.K. proposed the concept for this study and assisted in the interpretation of the results. E.G. performed the thermal wind analysis. E.G. and D.D. performed the Slepian approach calculations. D.R.B., W.M.F., and K.O. assisted with the data collection, processing, and analysis. S.J.B., S.M.L., L.N.F., T.G., R.H., L.I., and C.L. assisted with the interpretation of the results. M.H.W. acquired the Hubble observations and determined the GRS velocity profile. **Competing interests:** M.H.W. is also affiliated with the University of Michigan. **Data and materials availability:** The Juno gravity data are available in the NASA Planetary Data System at https://atmos.nmsu.edu/PDS/data/jnogrv_1001// DATA/RSR/; we used the files from 2016240 to 2019202. The geometry of the Juno orbit from 2016 to 2019, including SPK trajectory files and CK spacecraft attitude files, is available at https://naif.jpl.nasa.gov/pub/naif/JUNO/kernels/. The raw Hubble Space Telescope imaging data are available from the Mikulski Archive for Space Telescopes (MAST) at https://archive.stsci.edu/hst/search.php under proposal ID 15502; we used datasets iduy09mmq, iduy09mvq, iduy10n4q, and iduy15ooq. The velocity field derived from those images is available in HDF5 format at MAST (*32*). Distribution of the MONTE navigation code is restricted by the Export Administration Regulations of the US Department of Commerce. Eligible readers may request a copy of MONTE, under a license that does not permit redistribution, at https://montepy.jpl.nasa.gov/. The derived range-rate residuals for PJ1 to PJ21 and partial derivatives for sample GRS parameters are available at https://doi.org/10.5281/zenodo.4649459. Executable Matlab code for the thermal wind model, for both the mascon and Slepian approaches, is available at https://github.com/egalanti/TW_GRS_Slepians.

SUPPLEMENTARY MATERIALS

science.org/doi/10.1126/science.abf1396
Materials and Methods
Figs. S1 to S9
Tables S1 to S3
References (*34*–*36*)
Movie S1

6 October 2020; accepted 28 April 2021
Published online 28 October 2021
10.1126/science.abf1396

Science

The depth of Jupiter's Great Red Spot constrained by Juno gravity overflights

Marzia ParisiYohai KaspiEli GalantiDaniele DuranteScott J. BoltonSteven M. LevinDustin R. BuccinoLeigh N. FletcherWilliam M. FolknerTristan GuillotRavit HelledLuciano IessCheng LiKamal OudrhiriMichael H. Wong

Science, 374 (6570), • DOI: 10.1126/science.abf1396

Measuring the depth of Jupiter's storms
The atmosphere of Jupiter consists of bands of winds rotating at different rates, punctuated by giant storms. The largest storm is the Great Red Spot (GRS), which has persisted for more than a century. It has been unclear whether the storms are confined to a thin layer near the top of the atmosphere or if they extend deep into the planet. Bolton *et al*. used microwave observations from the Juno spacecraft to observe several storms and vortices. They found that the storms extended below the depths at which water and ammonia are expected to condense, implying a connection with the deep atmosphere. Parisi *et al*. analyzed gravity measurements taken while Juno flew over the GRS. They detected a perturbation in the planet's gravitational field caused by the storm, finding that it was no more than 500 kilometers deep. In combination, these results constrain how Jupiter's meteorology links to its deep interior. —KTS

View the article online
https://www.science.org/doi/10.1126/science.abf1396
Permissions
https://www.science.org/help/reprints-and-permissions